THE JOURNAL OF PHYSICAL CHEMISTRY C

Article

Cite This: J. Phys. Chem. C 2018, 122, 5566−5577

pubs.acs.org/JPCC

Adsorption of 1-Propanol in the Channel-Like InOF-1 Metal−Organic Framework and Its Influence on the CO_2 Capture Performances

J. Raziel Álvarez,[†,⊥] Paulo G. M. Mileo,[‡,⊥] Elí Sánchez-González,[†] J. Antonio Zárate,[†] Joelis Rodríguez-Hernández,[§] Eduardo González-Zamora,[∥] Guillaume Maurin,*[,‡] and Ilich A. Ibarra*[,†]

[†]Laboratorio de Fisicoquímica y Reactividad de Superficies (LaFReS), Instituto de Investigaciones en Materiales, Universidad Nacional Autónoma de México, Circuito Exterior s/n, CU, 04510 Delegación Coyoacán, Ciudad de México, Mexico

[‡]Institut Charles Gerhardt Montpellier, UMR-5253, Université de Montpellier, CNRS, ENSCM, Place E. Bataillon, 34095 Montpellier cedex 05, France

[§]Departamento de Materiales Avanzados, Centro de Investigación en Química Aplicada, Blvd. Enrique Reyna No. 140, 25294 Saltillo, Coahuila, Mexico

[∥]Departamento de Química, Universidad Autónoma Metropolitana-Iztapalapa, San Rafael Atlixco 186, Col. Vicentina, C. P. 09340 Delegación Iztapalapa, Ciudad de México, Mexico

Supporting Information

ABSTRACT: The *n*-PrOH adsorption properties of the one-dimensional-channel-like metal−organic framework InOF-1 were first explored and evidenced a high affinity for this host−guest system owing to the shape of the adsorption isotherms at a low relative pressure, the presence of a hysteresis loop during the desorption process, and a relatively high isosteric heat of adsorption. Monte Carlo simulations revealed that this thermodynamic behavior is related to a preferential interaction between *n*-PrOH and the μ_2-OH groups of the InOF-1 surface at low loading, whereas *n*-PrOH self-aggregates at higher guest concentration to first form dimers and then clusters. In complement to this thermodynamic exploration, the kinetics of *n*-PrOH were further characterized and the mobility of the guests was shown to be slow most probably due to the formation of these guest clusters. Finally, we revealed that in contrast to other solvents we have reported in the past, the *n*-PrOH confinement does not enhance the CO_2 capture in InOF-1. This observation was supported by grand canonical Monte Carlo simulations. Finally, we observed that the filling of the micropores of InOF-1 by CO_2 inhibits the adsorption of *n*-PrOH, demonstrating the absence of oversolubility of *n*-PrOH in the presence of CO_2.

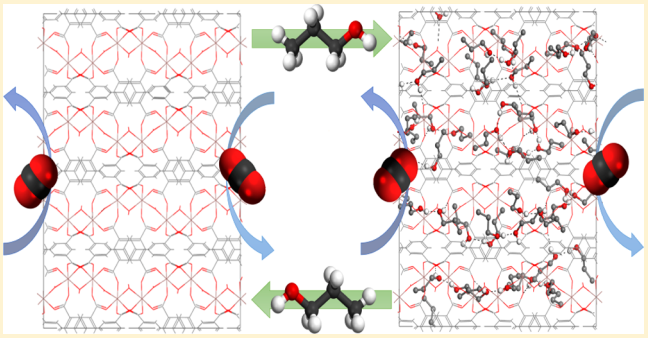

INTRODUCTION

Metal−organic frameworks (MOFs), a well-known class of crystalline hybrid porous three-dimensional materials, are constructed from metal ions and bridging organic ligands, which exhibit a huge collection of topologies.[1−5] Owing to the large diversity of the organic ligands and the high versatility of the inorganic building blocks, the design and construction of MOFs containing multifunctional sites and associated with a high chemical stability, has demonstrated the great potential of this family of porous materials in a large variety of fields.[6−9] Among them, energy-related applications from energy storage to transformation represent one of the most studied and promising research fields for MOFs.[10,11] Typically, MOFs have shown very interesting properties of H_2 storage,[12−14] CO_2 capture,[15−19] and diverse gas separations.[20−23] Recently, MOFs have been also suggested for adsorption-driven heat pump/chiller applications,[24−26] where the selection of a suitable working pair, i.e., working fluid (alcohol, water, ammonia) and adsorbent is, indeed, a key to design the optimal system. Interestingly, besides the thermodynamic adsorption capacity and affinity, the diffusivity of the working fluids through the pores of MOFs is of importance and experimental information is, however, still scarce.[27−29]

The confinement of guest molecules within the porous materials exemplifies a new and interesting approach to enhance their CO_2 capture performances.[30−32] The physical properties of guest molecules remarkably depend on the system scale; the confinement of these molecules within nanomaterials significantly transforms their density, viscosity, specific heat, and dielectric constant.[33−36] Uncommon confinement effects of the guest molecules located within the channels have been observed previously for single-walled carbon nanotubes.[37,38] However, these effects have been much scarcely investigated for MOFs materials.[39] For example, by confining large amounts of guest

Received: January 8, 2018
Revised: February 9, 2018
Published: February 13, 2018

DOI: 10.1021/acs.jpcc.8b00215
J. Phys. Chem. C 2018, 122, 5566−5577

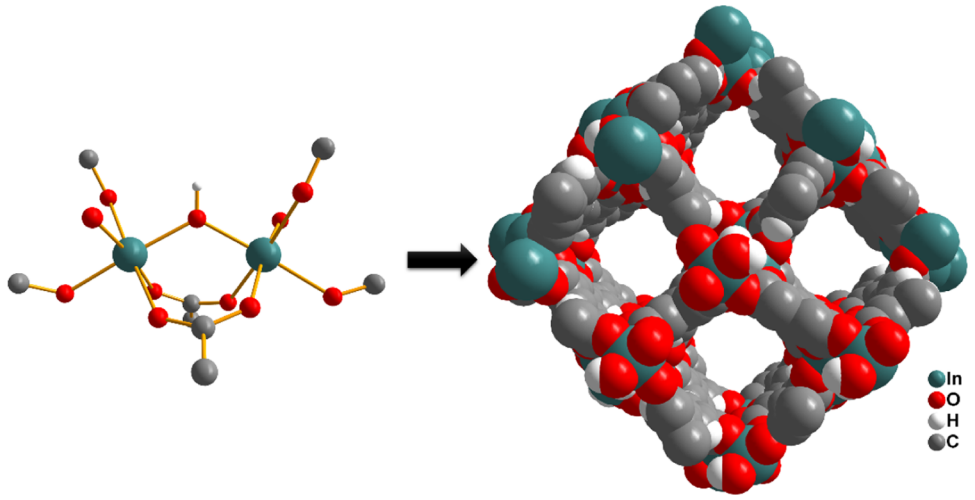

Figure 1. (Left) View of the binuclear building block of two metal ions oxygen octahedra bridged by a μ_2-hydroxyl group and (right) the crystal structure of InOF-1 along the *c*-axis showing channels of 7.50 Å pore dimension.

molecules (H_2O) in a mesoporous MOF material (MIL-100(Fe)), Llewellyn et al.[40] showed a 5-fold enhancement in the CO_2 capture. Conversely, Walton et al.[41−43] confined small amounts of H_2O within microporous MOF materials showing (i) augmented CO_2 capture performances of the corresponding MOFs and (ii) key role of the hydroxyl (−OH) functional groups in the interactions with H_2O to favor an efficient and ordered packing of the guests inside the pores. Our research groups have, systematically, confined small amounts of H_2O within microporous MOF materials to enhance their CO_2 capture capacities.[44,45] By taking the advantage of commensurate adsorption,[46] where the molecular size and shape of the guest molecule (e.g., H_2O) lead to a particular orientation that is compatible with the crystalline pore structure of the porous materials, these guest molecules can be accommodated more efficiently with a more ordered distribution.[47−49] Concisely, the hydroxyl (μ_2-OH) functional groups that are incorporated within the selected MOF materials (e.g., NOTT-400,[50] NOTT-401,[51] MIL-53(Al),[52] and InOF-1[53]) can "pin" H_2O via relatively strong hydrogen-bonding interactions.[54,55] In addition to H_2O, we investigated the confinement of different guest molecules, e.g., *N*,*N*-dimethylformamide (DMF),[56] EtOH,[57,58] MeOH,[59,60] and *i*-PrOH.[59] In this paper, we explore a complementary route via confining 1-propanol (*n*-PrOH) within the pores of InOF-1, an indium-based channel-like MOF of 7.50 Å pore dimension, with In(III) octahedral linked to four O-donors from four different $BPTC^{4-}$ ligands (H_4BPTC = biphenyl-3,3′,5,5′-tetracarboxylic acid)[61] and two μ_2-OH functional groups (Figure 1) to gain a full fundamental understanding of its solvent-controlled CO_2 adsorption performances. This joint experimental−computational study explores the influence of *n*-PrOH on the CO_2 adsorption performances of InOF-1 as compared to other solvents previously investigated. In addition to this, a special attention is dedicated to understand the adsorption and kinetic behaviors of *n*-PrOH in the pores of this MOF.

EXPERIMENTAL SECTION

Chemicals. Biphenyl-3,3′,5,5′-tetracarboxylic acid (H_4BPTC), indium nitrate ($In(NO_3)_3$), *N*,*N*-dimethylformamide (DMF), acetonitrile (CH_3CN), and nitric acid (65%, HNO_3) were acquired from Sigma-Aldrich and used as received.

Material Synthesis. InOF-1 = [$In_2(OH)_2$(BPTC), BPTC = biphenyl-3,3′,5,5′-tetracarboxylate] was synthesized following a previously reported recipe:[61] $In(NO_3)_3$ (156 mg, 0.40 mmol) and H_4BPTC (33 mg, 0.10 mmol) were mixed and dissolved in CH_3CN (5 mL), DMF (5 mL), and HNO_3 (65%, 0.2 mL) and finally sealed in a glass pressure tube. The clear solution was heated up at 358 K in an oil bath for 72 h. The pressure tube was cooled down to room temperature over a period of 12 h and the colorless crystalline product was separated by filtration, washed with DMF (5 mL), and dried in air, leading to a yield of 74% (based on ligand). Thermogravimetric analysis and powder X-ray diffraction were performed to control the nature and purity of the synthesized material (see the Supporting Information, Figures S1 and S2). The as-synthesized InOF-1 sample was acetone-exchanged and activated at 453 K for 2 h (either under 10^{-3} bar, static experiments, or with a constant flow of N_2 gas, dynamic experiments).

Adsorption Isotherms for N_2, CO_2, and *n*-PrOH. The N_2 sorption isotherms (77 K and up to 1 bar) were carried out on a Belsorp mini II analyzer under a high vacuum in a clean system with a diaphragm pumping system. The estimated Brunauer−Emmett−Teller area ($0.01 < P/P_0 < 0.04$) and pore volume were 1063 $m^2\ g^{-1}$ and 0.37 $cm^3\ g^{-1}$, respectively, consistent with previous findings for InOF-1.[60,61] Single-component CO_2 adsorption isotherms in the presence of *n*-PrOH up to 1 bar at 196 and 303 K were performed on a Belsorp HP (High Pressure) analyzer. Ultrapure grade (99.9995%) N_2 and CO_2 gases were purchased from Praxair. Single-component *n*-PrOH isotherms were recorded in a DVS Advantage 1 instrument from Surface Measurement System at 293 and 303 K.

Molecular Simulations. Grand canonical Monte Carlo (GCMC) simulations were carried out at 196 and 303 K to predict the adsorption isotherms for CO_2 as the single component and in mixture with 2 wt % *n*-PrOH in InOF-1 using a simulation box made of 8 (2 × 2 × 2) unit cells of the MOF (2 wt % *n*-PrOH corresponds to 6 molecules per simulation box). Additional MC simulations in the canonical (NVT) ensemble were performed at 303 K for *n*-PrOH as single component at low (1 molecule per simulation box), intermediate (6 and 24 molecules per simulation box), and high loading (47 molecules per simulation box corresponding to the experimental saturation capacity) to identify the most preferential sitting sites/

DOI: 10.1021/acs.jpcc.8b00215
J. Phys. Chem. C 2018, 122, 5566−5577

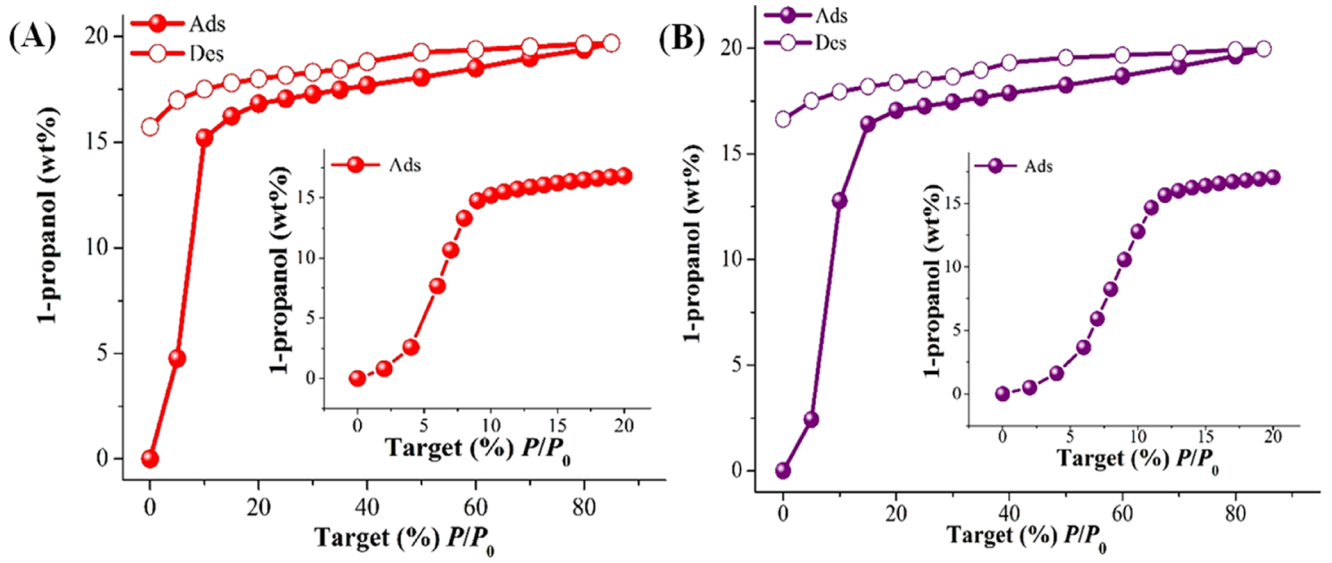

Figure 2. 1-Propanol (*n*-PrOH) adsorption isotherms of InOF-1 from % P/P_0 = 0−85 at 303 K (A) and 293 K (B). Solid and open circles correspond to the adsorption and desorption branches, respectively. The insets show the *n*-PrOH adsorption isotherms from % P/P_0 = 0−20.

interactions with the MOF pore wall, whereas the *n*-PrOH adsorption enthalpy at low coverage was simulated using the revised Widom's test particle insertion method.[62] The host−guest and guest−guest interactions were treated using a 12−6 Lennard-Jones (LJ) potential and Coulombic contributions. The EPM2[63] and united-atom TraPPE[64] models were selected for CO_2 and *n*-PrOH, respectively, whereas the atoms of the MOF framework were described by the LJ charged sites with parameters extracted from the generic force field UFF[65] and Dreiding[66] for the inorganic and organic nodes, respectively, and the partial charges taken from our previous study.[60] The Coulombic interactions were calculated using the Ewald summation technique with 10^{-6} precision and a 12 Å cutoff radius was considered to evaluate the short-range dispersion interactions. For each state point of these simulations, 2×10^7 Monte Carlo steps following 10^7 equilibration steps have been used. The analysis of the preferential interactions/locations of the guest species was performed through the plots of the radial distribution functions (RDFs) between different MOF/guest pairs and the center-of-mass distribution of the guests averaged over all of the configurations generated by MC simulations.

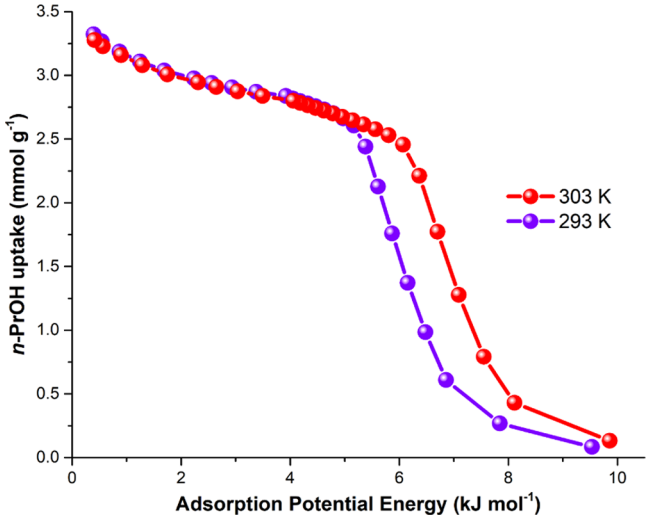

Figure 3. Plot of *n*-PrOH uptake as a function of ε (adsorption potential energy) at 293 K (violet) and 303 K (red).

RESULTS AND DISCUSSION

1-Propanol Sorption Studies. 1-Propanol (*n*-PrOH) sorption experiments were carried out on InOF-1. First, an acetone-exchanged InOF-1 sample was loaded into an analyzer cell (DVS Advantage 1 instrument) and activated at 453 K for 2 h. After the activation was completed, the analyzer cell (containing the activated InOF-1 sample) was cooled down to 303 K, and *n*-PrOH sorption isotherm was performed from % P/P_0 = 0−85 (Figure 2A). P_0 is the saturated vapor pressure of *n*-PrOH at the working temperature (2.02 and 3.86 kPa at 293 and 303 K, respectively). Figure 2A shows the *n*-PrOH isotherm at 303 K, where a steep increase in the *n*-PrOH uptake from % P/P_0 = 0 up to approximately % P/P_0 = 10 (15.20 *n*-PrOH wt %) was observed. From this pressure up to the end of the experiment (% P/P_0 = 85), the uptake slightly increases and reaches a quasi-plateau corresponding to a total amount of ∼19.70 *n*-PrOH wt %.

The sharp increase in the adsorption uptake of *n*-PrOH at low pressure indicates a relatively high affinity between InOF-1 and the guest molecule. In addition, the hysteresis loop observed along the desorption branch confirms this relatively strong host−guest interaction because this cannot be attributed to a "kinetic trapping" effect as suggested in other systems (see refs 67 and 68 for some representative examples). The so-called kinetic trap effect usually occurs when the pore dimensions of the adsorbent are close to the kinetic diameter (critical diameter) of the guest molecule. Here, as mentioned earlier, the pore dimension of InOF-1 (∼7.50 Å)[61] is significantly larger than the kinetic diameter of *n*-PrOH (4.7 Å).

The relatively high affinity between InOF-1 and *n*-PrOH was corroborated by the assessment of the isosteric heat of adsorption (ΔH = −53.30 kJ mol^{-1}, at low *n*-PrOH coverage), which was calculated from the adsorption isotherms measured at three different temperatures (303, 293, and 283 K) using the Clausius−Clapeyron equation (see the Supporting Information, Figures S3−S5).[69−71] This value is very well reproduced by the simulated adsorption enthalpy (−50.70 kJ mol^{-1}), and they both are higher than the molar enthalpy of vaporization for *n*-PrOH

DOI: 10.1021/acs.jpcc.8b00215
J. Phys. Chem. C 2018, 122, 5566−5577

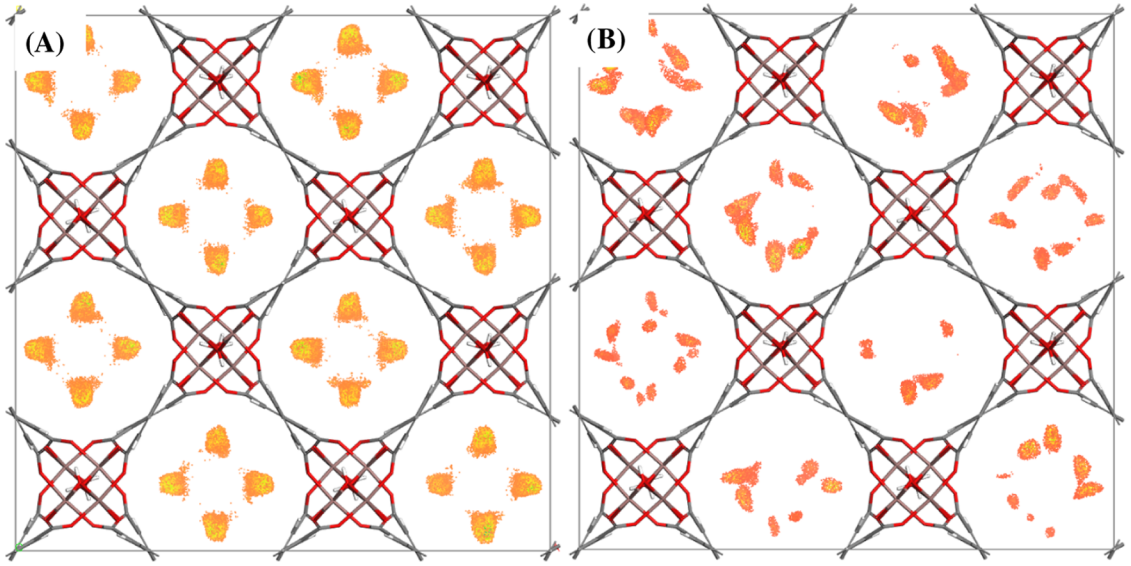

Figure 4. Center-of-mass distribution of *n*-PrOH in InOF-1 averaged over the Monte Carlo configurations obtained at 303 K for a loading of 1 guest molecule per simulation box (A) and 47 guest molecules per simulation box (B).

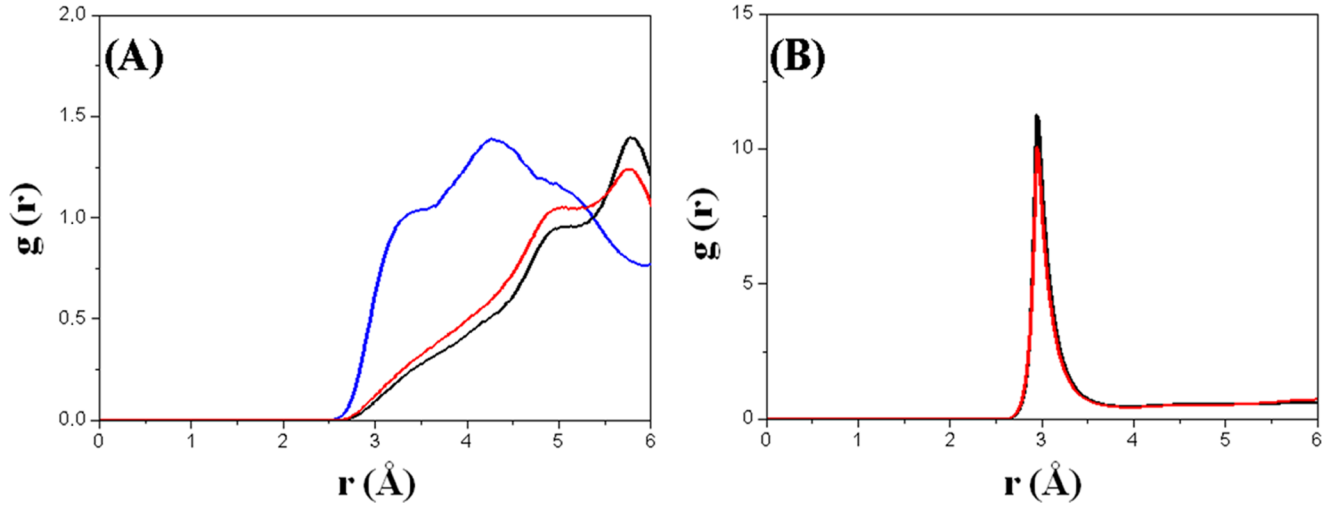

Figure 5. Radial distribution functions (RDFs) averaged over the Monte Carlo configurations at 303 K between (A) the oxygen atom of *n*-PrOH molecules and the oxygen atom of μ_2-OH of InOF-1 at low (1 guest molecule per simulation box, blue line), intermediate (6 guest molecules per simulation box, black line), and high loading (47 guest molecule per simulation box, red line). (B) The oxygen atoms of *n*-PrOH molecules at intermediate and high loadings.

(−47.45 kJ mol^{-1} at 298 K). It is worth mentioning that the so-obtained ΔH for *n*-PrOH is within the same range of value than those reported for the same molecule in μ_2-OH-containing MOFs.[72]

The *n*-PrOH sorption isotherm at 293 K is similar, as expected, to the adsorption−desorption experiment at 303 K (Figure 2B). The tiny dissimilarities are the total *n*-PrOH uptake (19.96 vs 19.68 *n*-PrOH wt %) and the hysteresis loop, which is slightly more pronounced. This behavior can be attributed to the fact that a lower operational temperature (293 K) might favor a more efficient packing of the *n*-PrOH guest molecules in the pores.

We further applied the Polanyi theory[73] to deeper understand the *n*-PrOH adsorption process within InOF-1. The adsorption potential energy (ε) represents the work required to change the states between *n*-PrOH in the adsorbed space to the adsorptive state. For one mole of an ideal gas, the potential theory establishes[73]

$$\varepsilon = \Delta F = \int_{P}^{P_0} V \, dP = RT \ln \frac{P_0}{P} \quad (1)$$

where ΔF is the free energy, V is the volume, and R is the universal gas constant equal to 8.3145 J K^{-1} mol^{-1}. The *n*-PrOH uptake as a function of the adsorption potential energy ε of InOF-1 (Figure 3) shows two distinct regions: first, at higher uptakes, the relationship is independent of the temperature and governed by the interactions between *n*-PrOH molecules themselves. This is related to a pore volume filling process, where the guest−guest interactions are dominant. The second region at low uptake shows a deviation between the curves at 293 and 303 K. This temperature-dependent profile is most probably associated with a relatively strong interaction between *n*-PrOH molecules and the pore wall of InOF-1.

To shed light on the adsorption behavior of *n*-PrOH at the microscopic scale, Monte Carlo simulations were performed at 303 K for different *n*-PrOH loading to identify their most

DOI: 10.1021/acs.jpcc.8b00215
J. Phys. Chem. C 2018, 122, 5566−5577

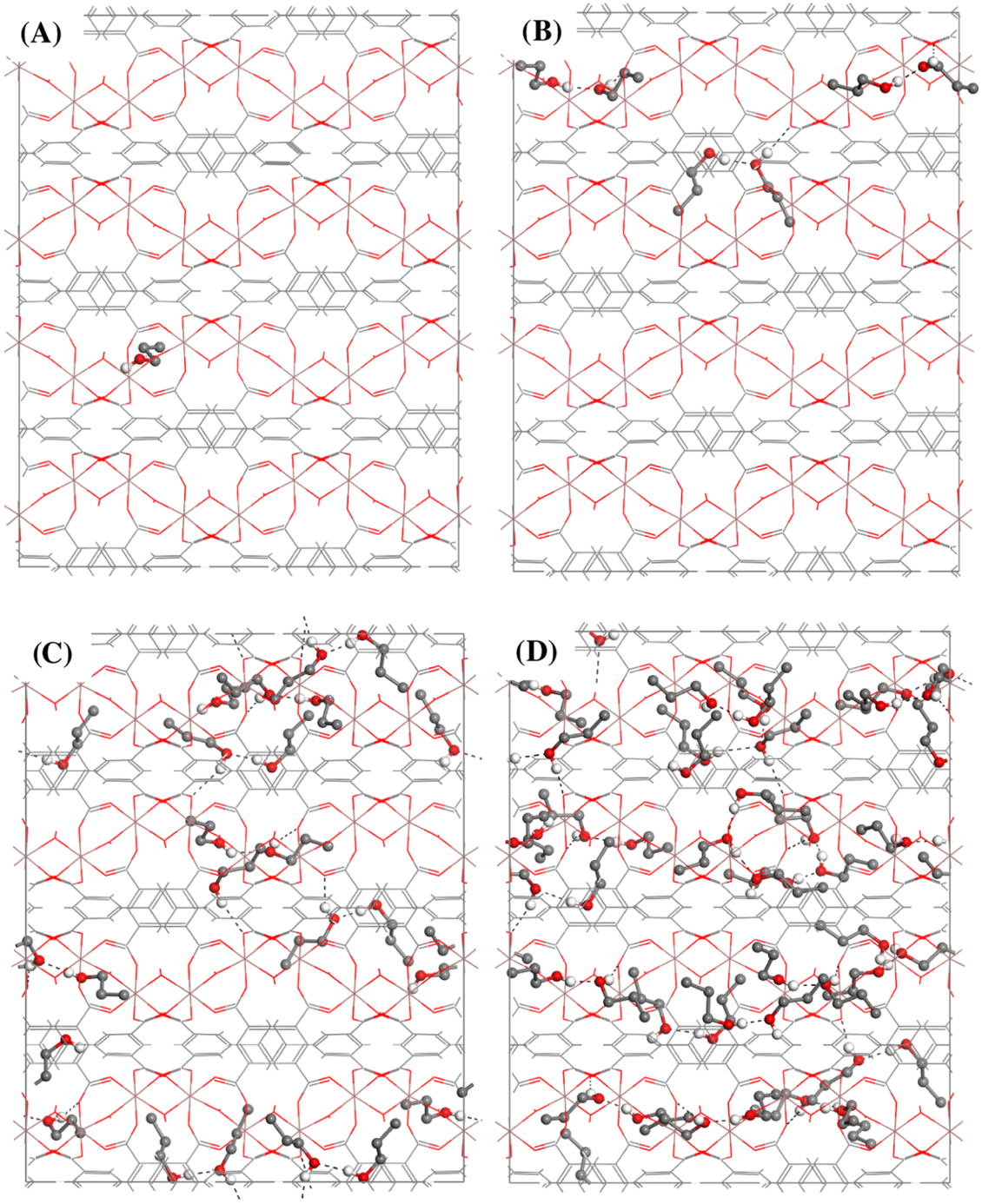

Figure 6. Monte Carlo configurations generated at 303 K showing different aggregation degrees of *n*-PrOH inside the pores of InOF-1 ((A), (B), (C), and (D) corresponding to 1, 6, 24, and 47 *n*-PrOH molecules per simulation box).

preferential adsorption sites and arrangements in the pores. The center-of-mass density map of *n*-PrOH plotted at low loading (Figure 4A) clearly supports a preferential interaction between *n*-PrOH and the μ_2-OH groups, as also evidenced by the presence of a shoulder at about 3.2 Å in the radial distribution function (RDF) for the corresponding $O_{\mu_2\text{-OH}}$−$O_{n\text{-PrOH}}$ pair (Figure 5A). When the loading increases, the location of *n*-PrOH is much less localized (Figure 4B) due to the *n*-PrOH−*n*-PrOH interactions as demonstrated by the sharp peak in the RDF for the corresponding $O_{n\text{-PrOH}}$−$O_{n\text{-PrOH}}$ pair (Figure 5B).

A further in-depth analysis of the MC configurations generated at different loadings revealed that when the loading increases, *n*-PrOH self-aggregates to first form dimers and then clusters (Figure 6).

Adsorption isobar experiments were further performed to characterize the sorption equilibrium phenomenon as a function of temperature.[74,75] Figure 7 shows that *n*-PrOH uptake increases with temperature. In zeolites and activated carbon materials it is characteristic to observe a decrease on gas and/or vapor uptake upon increasing temperature. However, for InOF-1 the n-PrOH adsorption isobar did not show such behavior.[76] This atypical behavior[75] of InOF-1 is most probably attributed to the need of overcoming a relatively high potential barrier to initiate the adsorption process. This is consistent with the

DOI: 10.1021/acs.jpcc.8b00215
J. Phys. Chem. C 2018, 122, 5566−5577

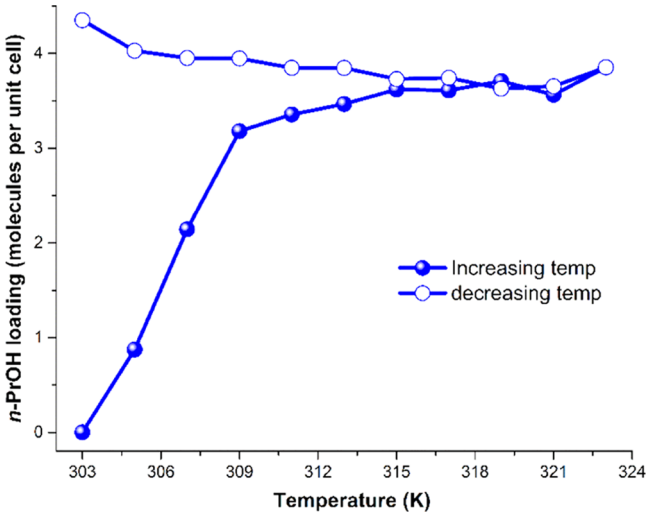

Figure 7. Sorption isobar plot of *n*-PrOH on InOF-1 at $0.02P/P_0$.

relatively strong interactions between *n*-PrOH molecules and the pore wall of InOF-1.

Experimental Kinetics Studies. The diffusion coefficient for *n*-PrOH, was further estimated by an uptake macroscopic method. Thus, a small amount of InOF-1 (~35 mg) was placed in a DVS Advantage 1 instrument to a step change in the partial pressure of *n*-PrOH (2, 5, 10, and 30% P/P_0), and adsorption was followed gravimetrically (Figure 8A). The diffusion coefficient was determined by matching the adsorption kinetic curves to the solution of diffusion equation for our boundary conditions. Considering (i) the small time regions, (ii) a diffusion coefficient independent of the position, (iii) a radial isothermal flux, and (iv) a constant *n*-PrOH concentration, the solution to the diffusion equation is equal to[77]

$$\frac{M_t}{M_\infty} \cong \frac{6}{r_p}\sqrt{\frac{\mathcal{D}t}{\pi}} - \frac{3\mathcal{D}t}{r_p^2} \text{ for } \frac{M_t}{M_\infty} < 0.8 \quad (2)$$

where M_t/M_∞ is the ratio of the amount adsorbed in time t and the mass adsorbed at infinite time (equilibrium adsorption mass), r_p is the experimental particle radius (see the Supporting Information), and $\mathcal{D}$ is the diffusion coefficient of *n*-PrOH. Due to the correlation between P/P_0 and the diffusion coefficient (Figure 8B), it is possible to refer this correlation as a transport diffusion phenomenon. In this diffusion process, the origin of the *n*-PrOH flux is due to the concentration gradient, i.e., the experimental boundary condition of the adsorbed molecules. In the low-pressure region, the main free path of the *n*-PrOH molecules considerably increases, so the probability of these molecules to collide with the pore walls is greater than that among themselves. This process is characterized by a very slow dynamic in the 0.02 and 0.05 P/P_0 region (see Figure 8B), where the diffusion coefficients were estimated to be 3.62×10^{-15} and 9.79×10^{-15} $cm^2\ s^{-1}$, respectively. These values are smaller in comparison to other MOFs (see the Supporting Information), which can be attributed to the strong host/guest interactions.

The diffusion regime within InOF-1 can be considered as configurational dynamics[77] due to the very slow mobility and strong concentration dependence (see Figure 8B). Thus, we can describe the dynamics of this guest as a combination of activated molecular jumps of *n*-PrOH between the preferential hydroxo functional groups and translational motions along the channel.

We can thus expect two mass transfer driving effects: (i) the preferential adsorption of *n*-PrOH molecules around the μ_2-OH groups of the InOF-1 and (ii) the cluster formation due to guest−guest interactions. Because the operational temperature is lower than the critical temperature of *n*-PrOH (T_c = 536.8 K), this leads to the possibility of dimers formation between the *n*-PrOH molecules as mentioned earlier based on our Monte Carlo predictions. Although it is expected that the aggregation of *n*-PrOH molecules induces a lower mobility than that of free *n*-PrOH molecules, the relatively small dimensions of the InOF-1 channels produce a constraint to the cluster formation. This constrain induces a high host−guest interaction and increases the main free path of the *n*-PrOH. For these reasons, we obtained an increase in the transport diffusion coefficients with P/P_0 (Figure 8B). Although an additional mass transfer resistance is probably due to the small crystallite dimensions of InOF-1 (see the Supporting Information, Figures S5−S6), we can expect a minimum intercrystalline resistance from the diffusion of adsorbed *n*-PrOH molecules through the particles because the observed particle size (see the Supporting Information, Figure S5) was relatively small.

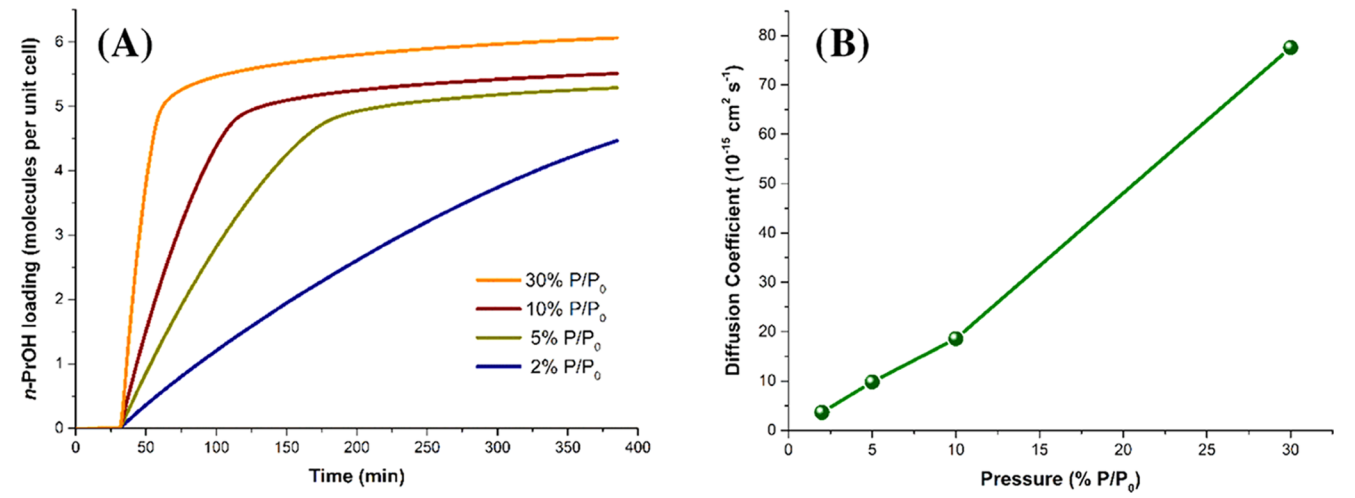

Figure 8. (A) Adsorption kinetics curves at different P/P_0 of *n*-PrOH in InOF-1. (B) Variation of transport diffusion coefficients of *n*-PrOH in InOF-1 at 303 K as a function of P/P_0 of *n*-PrOH.

DOI: 10.1021/acs.jpcc.8b00215
J. Phys. Chem. C 2018, 122, 5566−5577

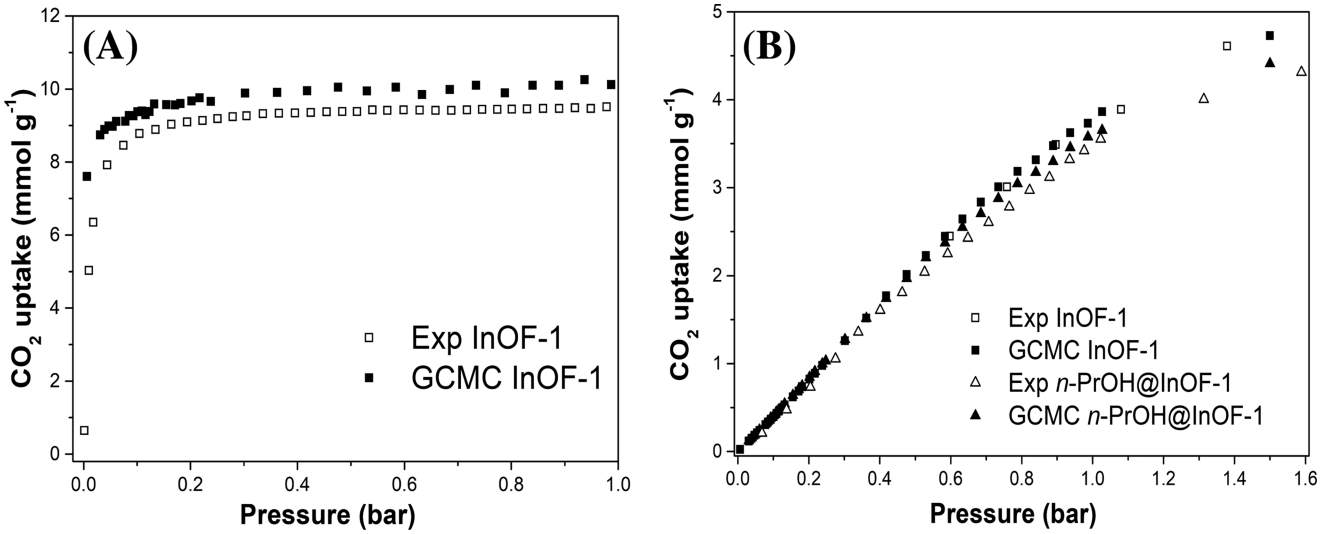

Figure 9. Experimental (empty symbols) and GCMC simulated (filled symbols) CO_2 adsorption isotherms of InOF-1 at 196 K (A) and of InOF-1 and *n*-PrOH@InOF-1 at 303 K (B).

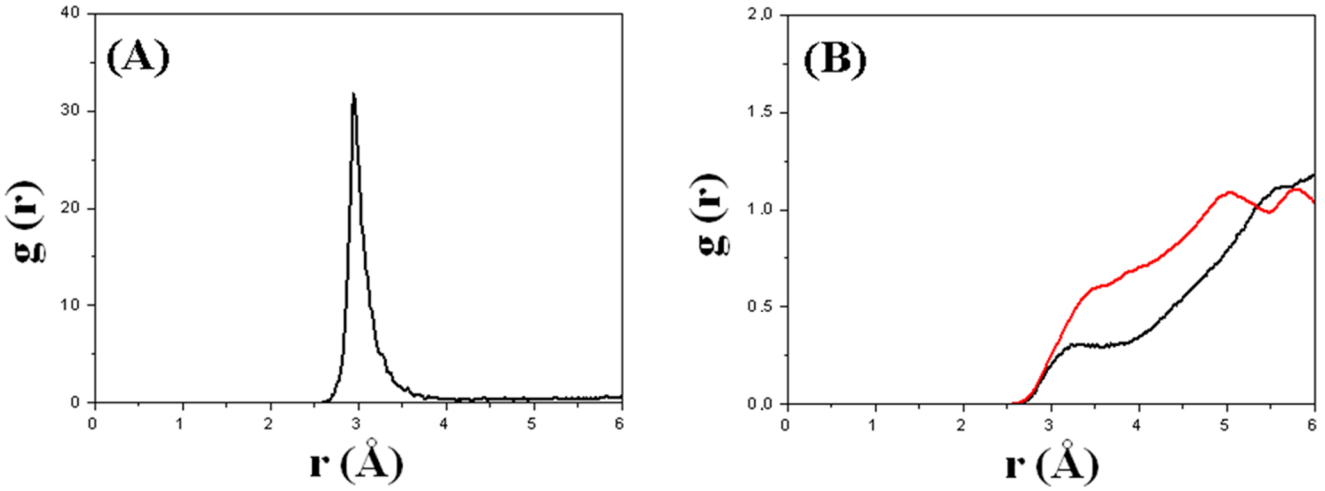

Figure 10. Radial distribution functions (RDFs) averaged over the grand canonical over the Monte Carlo configurations obtained at 303 K and 1 bar for the adsorption of CO_2 in *n*-PrOH@InOF-1 between (A) the oxygen atoms of *n*-PrOH molecules and (B) the oxygen atom of *n*-PrOH molecules (red line), the oxygen atom of CO_2 (black line), and the oxygen atom of μ_2-OH of InOF-1.

CO_2 Adsorptions Properties. An acetone-exchanged sample of InOF-1 was placed on a sample holder of a thermobalance Q500 HR and fully activated (453 K for 2 h and under a constant flow of N_2 of 60 mL min^{-1}), cooled down to 303 K (under N_2), and fully saturated with *n*-PrOH (see the Supporting Information). Later, by performing a specific activation protocol for this *n*-PrOH saturated sample (see the Supporting Information), the residual amount of confined *n*-PrOH was equal to 2 wt %. To confirm the reproducibility of this activation protocol for InOF-1, five different experiments were performed (see the Supporting Information), which corroborated the same residual (confined) amount of *n*-PrOH. Hereinafter, this sample will be referred to as *n*-PrOH@InOF-1.

First, to validate our modeling approach, we performed the CO_2 sorption experiments on a fully activated sample of InOF-1, which evidenced a total CO_2 uptake of 9.5 mmol g^{-1} (41.8 wt %) at 196 K (see Figure 9A). One observes a good agreement between the GCMC simulated and experimental adsorption isotherms, which validates the microscopic model and the force field parameters used to describe both the MOF structure and CO_2 and the MOF/CO_2 interactions. The CO_2 adsorption properties of *n*-PrOH@InOF-1 were then explored by performing static and isothermal CO_2 adsorption experiments at 303 K from 0 to 1 bar.

Static and dynamic (isothermal) CO_2 experiments on *n*-PrOH@InOF-1 samples did not show any improvement in the CO_2 capture (see Figure 9B and the Supporting Information, Figure S8). We reported earlier that by confining small amounts of H_2O,[53] EtOH,[57] MeOH,[60] and DMF[56] within the micropores of InOF-1, the CO_2 uptake was considerably enhanced. In this case, the confinement of *n*-PrOH did not augment the CO_2 adsorption properties of InOF-1. Interestingly, this trend was confirmed by our GCMC simulations at 303 K, which evidenced that the CO_2 amount adsorbed remains almost unchanged up to 0.6 bar and only slightly decreases up to 1 bar once InOF-1 is impregnated with 2 wt % of *n*-PrOH (see Figure 9B).

An in-depth analysis of the simulated preferential settings of *n*-PrOH and CO_2 in a mixture evidenced that in contrast to MeOH, which was predicted to form well-localized single adducts with the μ_2-OH groups, *n*-PrOH tends to preferentially

DOI: 10.1021/acs.jpcc.8b00215
J. Phys. Chem. C 2018, 122, 5566−5577

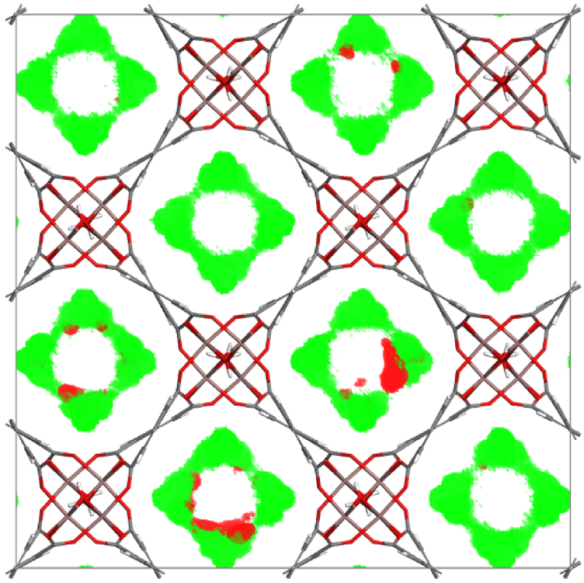

Figure 11. Center-of-mass distribution of CO_2 (green) and *n*-PrOH (red) in *n*-PrOH@InOF-1 averaged over the Monte Carlo configurations obtained at 303 K and 1 bar.

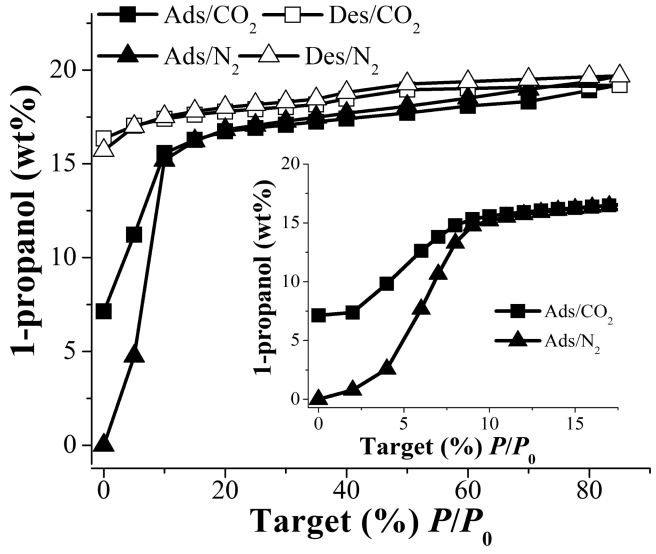

Figure 13. *n*-PrOH adsorption isotherms at 303 K of InOF-1 from % P/P_0 = 0−85 with two different gas carriers: solid triangles correspond to the N_2 carrier (100 mL min^{-1}); solid squares correspond to the CO_2 carrier (100 mL min^{-1}). Solid symbols represent adsorption and open symbols show desorption. The inset shows the *n*-PrOH adsorption isotherms (N_2 and CO_2 carriers) at 303 K from % P/P_0 = 0−18.

form clusters in a similar way than for the single-component adsorption of *n*-PrOH, leading to much weaker interactions between this guest and the μ_2-OH groups. This is illustrated in the RDFs plotted in Figure 10 at 1 bar and 303 K, which clearly show the presence of a sharp peak for the $O_{n\text{-PrOH}}$−$O_{n\text{-PrOH}}$ pair at a relatively short distance of 2.95 Å (Figure 10A), characteristic of a relatively strong hydrogen bond association of the *n*-PrOH molecules, whereas the probability of the *n*-PrOH/μ_2-OH interactions is much lower (Figure 10B).

The center-of-mass density map of both guest molecules *n*-PrOH@InOF-1 plotted in Figure 11 for the *n*-PrOH@InOF-1 system confirms a much less localized setting of *n*-PrOH as compared to MeOH and this leads to a much higher degree of blocking of the pores.

This is further illustrated in the van der Waals surface plot obtained for *n*-PrOH@InOF-1 (Figure 12), which evidences that the organization of *n*-PrOH in the pores leads to a significant decrease in the accessible porosity by creating an exclusion zone for the adsorption of CO_2. This scenario, which is consistent with a decrease in the CO_2 uptake for *n*-PrOH@InOF-1, strongly differs with that of MeOH@InOF-1, for which we previously evidenced a more localized distribution of the guest, leading to the formation of a lump at the vicinity of the μ_2-OH groups, thus increasing the confinement effect and an increase in the CO_2 uptake.[60]

Although the confinement of *n*-PrOH did not enhance the CO_2 capture properties of InOF-1, it provided us the curiosity of exploring a different alternative. Certainly, we have previously

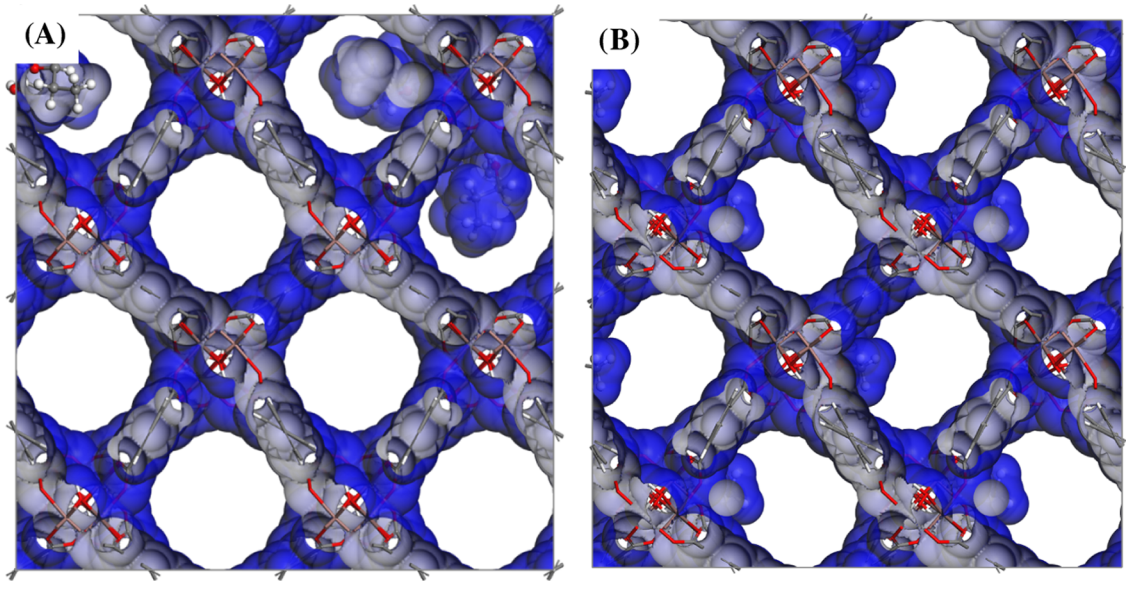

Figure 12. Comparison of the van der Waals surface plots of the *n*-PrOH@InOF-1 (A) and the MeOH@InOF-1 (B).

DOI: 10.1021/acs.jpcc.8b00215
J. Phys. Chem. C 2018, 122, 5566−5577

demonstrated that the confinement of small amounts of polar solvents in microporous MOFs can considerably enhance the CO_2 capture.[44,45] Conversely, when large amounts of these solvents were confined, the CO_2 capture properties were drastically diminished.[53,56,57] Up to this point, we have only investigated the confinement of polar solvents within InOF-1 to enhance the capture of CO_2. But what about the other way round? Indeed, the physicochemical properties in nanometer confining porous scales of condensed matter are considerably different to what is observed at the macroscopic level. Some recent investigations have demonstrated that the confinement of solvents in porous materials considerably enhances the gas solubility. This improvement is known as "oversolubility".[78−81] The oversolubility of confined solvents considerably modifies their viscosity, density, dielectric constant, and specific heat.[37,38] As an example, Garcia-Garibay[82] showed in a MOF material entitled UCLA-R3 that the confinement of DMF significantly enhanced the viscosity of this solvent up to 4 orders of magnitude.

Thus, we investigated the feasibility of confining CO_2 (within the micropores of InOF-1) to oversolubilize *n*-PrOH. First, we placed an acetone-exchanged sample of InOF-1 into an analyzer cell (DVS Advantage 1 instrument). This sample was fully activated (453 K for 2 h) and the temperature reduced to 303 K to carry out a *n*-PrOH adsorption isotherm from % P/P_0 = 0−85 (Figure 13). The particularity of this experiment was the use of CO_2 as a carrier (100 mL min^{-1}) of *n*-PrOH vapor. For comparison, we also reported the *n*-PrOH adsorption isotherm performed with N_2 (solid triangles) as a carrier (100 mL min^{-1}). Thus, the first interesting phenomenon occurs at the low loading of *n*-PrOH (from 0 to approximately 10% P/P_0), where the isotherms using either CO_2 or N_2 as carriers significantly differ (see the inset of Figure 13). The material is initially saturated with the corresponding gas carrier. When using N_2 at 303 K, it has been already demonstrated that InOF-1 did adsorb small amounts of this guest at 1 bar and, thus, the material can be considered as an empty InOF-1.[53] Conversely, when using CO_2, the total uptake at 303 K and 1 bar was approximately 7.1 wt % (see the inset of Figure 13).

This scenario where the micropores of InOF-1 are saturated by CO_2 can prove if confined CO_2 is able to further oversolubilize *n*-PrOH. Figure 13 shows that this adsorption isotherm significantly deviates with that obtained upon N_2 carrier in the range of relative pressure 0−10% P/P_0 (Figure 13). By adjusting the mathematical equations to both isotherms in this low domain of pressure, we can describe the adsorption behavior of InOF-1 in these two situations, and the slope of these equations can indicate the affinity of *n*-PrOH toward the material under different gas carriers (see the Supporting Information, Figure S9). Based on this, we observe a steeper slope and indeed a higher affinity for the adsorption of *n*-PrOH for the N_2-carrier InOF-1 (corresponding to the empty InOF-1) than for the CO_2-carrier InOF-1. This result suggests that when the micropores of InOF-1 are filled with CO_2 molecules, this makes more complex the adsorption of *n*-PrOH molecules. At a higher relative pressure from 10 to 85% P/P_0, the isotherms of N_2-carrier InOF-1 and CO_2-carrier InOF-1 (Figure 13) reached the same maximum amount of *n*-PrOH adsorbed, demonstrating that there is no oversolubility effect of *n*-PrOH in CO_2.

CONCLUSIONS

The exploration of the adsorption behavior of *n*-PrOH in the channel-like MOF InOF-1 evidences a relatively strong host−guest interaction that led to a sudden increase in the adsorption isotherm at low pressure, as well as the presence of a hysteresis loop during the desorption process. This experimental evidence was supported by macroscopic and microscopic modeling, typically Monte Carlo simulations revealed that *n*-PrOH preferentially sits around the μ_2-OH groups of InOF-1 at low alcohol loading, while *n*-PrOH self-aggregates to first form dimers and then clusters at higher loading. It was further shown that the adsorption kinetics of this guest is slow due to the confinement and the aggregation of the molecules.

From previous studies in this material, we have demonstrated the improvement in the CO_2 adsorption capacity by the formation of a well-localized single adducts between polar molecules and μ_2-OH groups ("bottleneck effect"). However, here the *n*-PrOH confinement did not enhance the CO_2 capture in InOF-1. This trend was also confirmed by GCMC simulations, which revealed that the preferential distribution of *n*-PrOH in mixture with CO_2 considerably decreases the accessibility of the porosity by creating an exclusion zone for the adsorption of CO_2. Finally, we explored the possibility of confining CO_2 to oversolubilize *n*-PrOH. Our results showed that when the micropores of InOF-1 are filled with CO_2, this inhibits the adsorption of *n*-PrOH, demonstrating the absence of oversolubility of *n*-PrOH in the presence of CO_2.

ASSOCIATED CONTENT

Supporting Information

The Supporting Information is available free of charge on the ACS Publications website at DOI: 10.1021/acs.jpcc.8b00215.

Thermogravimetric analysis, sample preparation and activation of InOF-1, isosteric enthalpy of adsorption calculations, scanning electron micrograph, affinity determination, and carbon dioxide diffusion are provided (PDF)

AUTHOR INFORMATION

Corresponding Authors

*E-mail: guillaume.maurin@univ-montp2.fr (G.M.).
*E-mail: argel@unam.mx. Fax: +52(55) 5622-4595 (I.A.I.).

ORCID

Elí Sánchez-González: 0000-0002-5440-329X
Guillaume Maurin: 0000-0002-2096-0450
Ilich A. Ibarra: 0000-0002-8573-8033

Author Contributions

⊥J.R.Á. and P.G.M.M. contributed equally to this work.

Author Contributions

The manuscript was written through contributions of all of the authors. All of the authors have given approval to the final version of the manuscript.

Notes

The authors declare no competing financial interest.

ACKNOWLEDGMENTS

The authors thank Dr. A. Tejeda-Cruz (powder X-ray; IIM-UNAM), CONACyT Mexico (1789), PAPIIT UNAM Mexico (IN101517) for financial support. E.G.-Z. thanks CONACyT (236879), Mexico for financial support. Thanks to U. Winnberg (ITAM) for scientific discussions. P.G.M.M. thanks the National Council of Technological and Scientific Development (CNPQ) for the scholarship. G.M. thanks the Institut Universitaire de France for its support. J.R.Á. acknowledges CONACyT Mexico

DOI: 10.1021/acs.jpcc.8b00215
J. Phys. Chem. C 2018, 122, 5566−5577

(Grant No. 276862). E.S.-G. thanks CONACyT Mexico (Grant No. 289042).

REFERENCES

(1) Hoskins, B. F.; Robson, R. Infinite Polymeric Frameworks Consisting of Three Dimensionally Linked Rod-Like Segments. *J. Am. Chem. Soc.* **1989**, *111*, 5962−5964.

(2) Kondo, M.; Yoshitomi, T.; Matsuzaka, H.; Kitagawa, S.; Seki, K. Three-Dimensional Framework with Channeling Cavities for Small Molecules: $\{[M_2(4,4'\text{-bpy})_3(NO_3)_4]\cdot xH_2O\}_n$ (M = Co, Ni, Zn). *Angew. Chem., Int. Ed.* **1997**, *36*, 1725−1727.

(3) Férey, G. Microporous Solids: From Organically Templated Inorganic Skeletons to Hybrid Frameworks... Ecumenism in Chemistry. *Chem. Mater.* **2001**, *13*, 3084−3098.

(4) Rowsell, J. L. C.; Yaghi, O. M. Metal−organic Frameworks: A New Class of Porous Materials. *Microporous Mesoporous Mater.* **2004**, *73*, 3−14.

(5) Férey, G. Hybrid Porous Solids: Past, Present, Future. *Chem. Soc. Rev.* **2008**, *37*, 191−214.

(6) Kuppler, R. J.; Timmons, D. J.; Fang, Q.-R.; Li, J.-R.; Makal, T. A.; Young, M. D.; Yuan, D.; Zhao, D.; Zhuang, W.; Zhou, H.-C. Potential Applications of Metal-Organic Frameworks. *Coord. Chem. Rev.* **2009**, *253*, 3042−3066.

(7) Czaja, A. U.; Trukhan, N.; Müller, U. Industrial Applications of Metal−organic Frameworks. *Chem. Soc. Rev.* **2009**, *38*, 1284−1293.

(8) Sánchez-Serratos, M.; Álvarez, J. R.; González-Zamora, E.; Ibarra, I. A. Porous Coordination Polymers (PCPs): New Platforms for Gas Storage. *J. Mex. Chem. Soc.* **2016**, *60*, 43−57.

(9) Maurin, G.; Serre, C.; Cooper, A.; Férey, G. The New Age of MOFs and of Their Porous-Related Solids. *Chem. Soc. Rev.* **2017**, *46*, 3104−3107.

(10) Li, S.-L.; Xu, Q. Metal−Organic Frameworks as Platforms for Clean Energy. *Energy Environ. Sci.* **2013**, *6*, 1656−1683.

(11) Bon, V. Metal-Organic Frameworks for Energy-Related Applications. *Curr. Opin. Green Sustainable Chem.* **2017**, *4*, 44−49.

(12) Dincă, M.; Long, J. R. Hydrogen Storage in Microporous Metal-Organic Frameworks with Exposed Metal Sites. *Angew. Chem., Int. Ed.* **2008**, *47*, 6766−6779.

(13) Thomas, K. M. Adsorption and Desorption of Hydrogen on Metal-Organic Framework Materials for Storage Applications: Comparison with Other Nanoporous Materials. *Dalton Trans.* **2009**, 1487−1505.

(14) Langmi, H. W.; Ren, J.; North, B.; Mathe, M.; Bessarabov, D. Hydrogen Storage in Metal-Organic Frameworks: A Review. *Electrochim. Acta* **2014**, *128*, 368−392.

(15) Hou, L.; Shi, W.-J.; Wang, Y.-Y.; Guo, Y.; Jin, C.; Shi, Q.-Z. A Rod Packing Microporous Metal-Organic Framework: Unprecedented *ukv* Topology, High Sorption Selectivity and Affinity for CO_2. *Chem. Commun.* **2011**, *47*, 5464−5466.

(16) Sumida, K.; Rogow, D. L.; Mason, J. A.; McDonald, T. M.; Bloch, E. D.; Herm, Z. R.; Bae, T.-H.; Long, J. R. Carbon Dioxide Capture in Metal−Organic Frameworks. *Chem. Rev.* **2012**, *112*, 724−781.

(17) Liu, J.; Thallapally, P. K.; McGrail, B. P.; Brown, D. R.; Liu, J. Progress in Adsorption-Based CO_2 Capture by Metal-Organic Frameworks. *Chem. Soc. Rev.* **2012**, *41*, 2308−2322.

(18) Wang, H.-H.; Hou, L.; Li, Y.-Z.; Jiang, C.-Y.; Wang, Y.-Y.; Zhu, Z. Porous MOF with Highly Efficient Selectivity and Chemical Conversion for CO_2. *ACS Appl. Mater. Interfaces* **2017**, *9*, 17969−17976.

(19) Li, X.-Y.; Li, Y.-Z.; Yang, Y.; Hou, L.; Wang, Y.-Y.; Zhu, Z. Efficient Light Hydrocarbon Separation and CO_2 Capture and Conversion in a Stable MOF with Oxalamide-Decorated Polar Tubes. *Chem. Commun.* **2017**, *53*, 12970−12973.

(20) Li, J.-R.; Kuppler, R. J.; Zhou, H.-C. Selective Gas Adsorption and Separation in Metal-Organic Frameworks. *Chem. Soc. Rev.* **2009**, *38*, 1477−1504.

(21) Li, J.-R.; Sculley, J.; Zhou, H.-C. Metal−Organic Frameworks for Separations. *Chem. Rev.* **2012**, *112*, 869−932.

(22) Adil, K.; Belmabkhout, Y.; Pillai, R. S.; Cadiau, A.; Bhatt, P. M.; Assen, A. H.; Maurin, G.; Eddaoudi, M. Gas/Vapour Separation Using Ultra-Microporous Metal-Organic Frameworks: Insights into the Structure/Separation Relationship. *Chem. Soc. Rev.* **2017**, *46*, 3402−3430.

(23) Cadiau, A.; Belmabkhout, Y.; Adil, K.; Bhatt, P. M.; Pillai, R. S.; Shkurenko, A.; Martineau-Corcos, C.; Maurin, G.; Eddaoudi, M. Hydrolytically Stable Fluorinated Metal-Organic Frameworks for Energy-Efficient Dehydration. *Science* **2017**, *356*, 731−735.

(24) Henninger, S. K.; Jeremias, F.; Kummer, H.; Janiak, C. MOFs for Use in Adsorption Heat Pump Processes. *Eur. J. Inorg. Chem.* **2012**, *2012*, 2625−2634.

(25) Cadiau, A.; Lee, J. S.; Damasceno Borges, D.; Fabry, P.; Devic, T.; Wharmby, M. T.; Martineau, C.; Foucher, D.; Taulelle, F.; Jun, C.-H.; et al. Design of Hydrophilic Metal Organic Framework Water Adsorbents for Heat Reallocation. *Adv. Mater.* **2015**, *27*, 4775−4780.

(26) Henninger, S. K.; Ernst, S. J.; Gordeeva, L.; Bendix, P.; Fröhlich, D.; Grekova, A. D.; Bonaccorsi, L.; Aristov, Y.; Jaenchen, J. New Materials for Adsorption Heat Transformation and Storage. *Renewable Energy* **2017**, *110*, 59−68.

(27) Jobic, H.; Rosenbach, N.; Ghoufi, A.; Kolokolov, D. I.; Yot, P. G.; Devic, T.; Serre, C.; Férey, G.; Maurin, G. Unusual Chain-Length Dependence of the Diffusion of *n*-Alkanes in the Metal-Organic Framework MIL-47(V): The Blowgun Effect. *Chem. - Eur. J.* **2010**, *16*, 10337−10341.

(28) Canepa, P.; Nijem, N.; Chabal, Y. J.; Thonhauser, T. Diffusion of Small Molecules in Metal Organic Framework Materials. *Phys. Rev. Lett.* **2013**, *110*, No. 026102.

(29) Yu, Z.; Deschamps, J.; Hamon, L.; Karikkethu Prabhakaran, P.; Pré, P. Modeling Hydrogen Diffusion in Hybrid Activated Carbon-MIL-101(Cr) Considering Temperature Variations and Surface Loading Changes. *Microporous Mesoporous Mater.* **2017**, *248*, 72−83.

(30) Ho, N. L.; Porcheron, F.; Pellenq, R. J.-M. Experimental and Molecular Simulation Investigation of Enhanced CO_2 Solubility in Hybrid Adsorbents. *Langmuir* **2010**, *26*, 13287−13296.

(31) Ho, L. N.; Perez Pellitero, J.; Porcheron, F.; Pellenq, R. J.-M. Enhanced CO_2 Solubility in Hybrid MCM-41: Molecular Simulations and Experiments. *Langmuir* **2011**, *27*, 8187−8197.

(32) Ho, N. L.; Perez-Pellitero, J.; Porcheron, F.; Pellenq, R. J.-M. Enhanced CO_2 Solubility in Hybrid Adsorbents: Optimization of Solid Support and Solvent Properties for CO_2 Capture. *J. Phys. Chem. C* **2012**, *116*, 3600−3607.

(33) Volino, F.; Gérard, H.; Miachon, S. Non-Extensive Visco-Elastic Theory II. First Experimental Tests of the Simple Theory with Rotational Modes. *Ann. Phys.* **1997**, *22*, 43−82.

(34) Morishige, K.; Shikimi, M. Adsorption Hysteresis and Pore Critical Temperature in a Single Cylindrical Pore. *J. Chem. Phys.* **1998**, *108*, 7821−7824.

(35) Kimball, M. O.; Gasparini, F. M. Universality and Finite-Size Scaling of the Specific Heat of ^{3}He−^{4}He Mixtures. *Phys. Rev. Lett.* **2005**, *95*, No. 165701.

(36) Zammit, U.; Marinelli, M.; Mercuri, F.; Paoloni, S. Effect of Confinement and Strain on the Specific Heat and Latent Heat over the Nematic−Isotropic Phase Transition of 8CB Liquid Crystal. *J. Phys. Chem. B* **2009**, *113*, 14315−14322.

(37) Hernández-Rojas, J.; Calvo, F.; Bretón, J.; Gomez Llorente, J. M. Confinement Effects on Water Clusters Inside Carbon Nanotubes. *J. Phys. Chem. C* **2012**, *116*, 17019−17028.

(38) Chakraborty, S.; Kumar, H.; Dasgupta, C.; Maiti, P. K. Confined Water: Structure, Dynamics, and Thermodynamics. *Acc. Chem. Res.* **2017**, *50*, 2139−2146.

(39) Jayasinghe, A. S.; Unruh, D. K.; Kral, A.; Libo, A.; Forbes, T. Z. Structural Features in Metal−Organic Nanotube Crystals That Influence Stability and Solvent Uptake. *Cryst. Growth Des.* **2015**, *15*, 4062−4070.

(40) Soubeyrand-Lenoir, E.; Vagner, C.; Yoon, J. W.; Bazin, P.; Ragon, F.; Hwang, Y. K.; Serre, C.; Chang, J. S.; Llewellyn, P. L. How Water Fosters a Remarkable 5-Fold Increase in Low-Pressure CO_2 Uptake within Mesoporous MIL-100(Fe). *J. Am. Chem. Soc.* **2012**, *134*, 10174−10181.

DOI: 10.1021/acs.jpcc.8b00215
J. Phys. Chem. C 2018, 122, 5566−5577

(41) Jasuja, H.; Huang, Y.; Walton, K. S. Adjusting the Stability of Metal−Organic Frameworks under Humid Conditions by Ligand Functionalization. *Langmuir* **2012**, *28*, 16874−16880.
(42) Jasuja, H.; Zang, J.; Sholl, D. S.; Walton, K. S. Rational Tuning of Water Vapor and CO_2 Adsorption in Highly Stable Zr-Based MOFs. *J. Phys. Chem. C* **2012**, *116*, 23526−23532.
(43) DeCoste, J. B.; Peterson, G. W.; Jasuja, H.; Glover, T. G.; Huang, Y.; Walton, K. S. Stability and Degradation Mechanisms of Metal−Organic Frameworks Containing the $Zr_6O_4(OH)_4$ Secondary Building Unit. *J. Mater. Chem. A* **2013**, *1*, 5642−5650.
(44) González-Zamora, E.; Ibarra, I. A. CO_2 Capture Under Humid Conditions in Metal−Organic Frameworks. *Mater. Chem. Front.* **2017**, *1*, 1471−1484.
(45) Benoit, V.; Chanut, N.; Pillai, R. S. S.; Benzaqui, M.; Beurroies, I.; Davautour-Vinot, S.; Serre, C.; Steunou, N.; Maurin, G.; Llewellyn, P. L. A Promising Metal-Organic Framework (MOF), MIL-96(Al) for CO_2 Separation Under Humid Conditions. *J. Mater. Chem. A* **2018**, 2081−2090.
(46) Wu, H.; Gong, Q.; Olson, D. H.; Li, J. Commensurate Adsorption of Hydrocarbons and Alcohols in Microporous Metal Organic Frameworks. *Chem. Rev.* **2012**, *112*, 836−868.
(47) Olson, D. H.; Kokotailo, G. T.; Lawton, S. L.; Meier, W. M. Crystal Structure and Structure-Related Properties of ZSM-5. *J. Phys. Chem.* **1981**, *85*, 2238−2243.
(48) Smit, B.; Maesen, T. L. M. Commensurate 'freezing' of Alkanes in the Channels of a Zeolite. *Nature* **1995**, *374*, 42−44.
(49) Olson, D.; Lan, A.; Seidel, J.; Li, K.; Li, J. Metal Organic Frameworks Showing Hydrocarbon Adsorption Properties Commensurate with Their Pore Structure. *Adsorption* **2010**, *16*, 559−565.
(50) Álvarez, J. R.; Peralta, R. A.; Balmaseda, J.; González-Zamora, E.; Ibarra, I. A. Water Adsorption Properties of a Sc(III) Porous Coordination Polymer for CO_2 Capture Applications. *Inorg. Chem. Front.* **2015**, *2*, 1080−1084.
(51) Sánchez-González, E.; Álvarez, J. R.; Peralta, R. A.; Campos-Reales-Pineda, A.; Tejeda-Cruz, A.; Lima, E.; Balmaseda, J.; González-Zamora, E.; Ibarra, I. A. Water Adsorption Properties of NOTT-401 and CO_2 Capture under Humid Conditions. *ACS Omega* **2016**, *1*, 305−310.
(52) Sánchez-Serratos, M.; Bayliss, P. A.; Peralta, R. A.; González-Zamora, E.; Lima, E.; Ibarra, I. A. CO_2 Capture in the Presence of Water Vapour in MIL-53(Al). *New J. Chem.* **2016**, *40*, 68−72.
(53) Peralta, R. A.; Alcántar-Vázquez, B.; Sánchez-Serratos, M.; González-Zamora, E.; Ibarra, I. A. Carbon Dioxide Capture in the Presence of Water Vapour in InOF-1. *Inorg. Chem. Front.* **2015**, *2*, 898−903.
(54) Burtch, N. C.; Jasuja, H.; Walton, K. S. Water Stability and Adsorption in Metal−Organic Frameworks. *Chem. Rev.* **2014**, *114*, 10575−10612.
(55) Cmarik, G. E.; Kim, M.; Cohen, S. M.; Walton, K. S. Tuning the Adsorption Properties of UiO-66 via Ligand Functionalization. *Langmuir* **2012**, *28*, 15606−15613.
(56) Sánchez-González, E.; González-Zamora, E.; Martínez-Otero, D.; Jancik, V.; Ibarra, I. A. Bottleneck Effect of *N*,*N*-Dimethylformamide in InOF-1: Increasing CO_2 Capture in Porous Coordination Polymers. *Inorg. Chem.* **2017**, *56*, 5863−5872.
(57) Peralta, R. A.; Campos-Reales-Pineda, A.; Pfeiffer, H.; Álvarez, J. R.; Zárate, J. A.; Balmaseda, J.; González-Zamora, E.; Martínez, A.; Martínez-Otero, D.; Jancik, V.; et al. CO_2 Capture Enhancement in InOF-1 via a Bottleneck Effect of Confined Ethanol. *Chem. Commun.* **2016**, *52*, 10273−10276.
(58) Álvarez, J. R.; Sánchez-Gonzalez, E.; Pérez, E.; Schneider-Revueltas, E.; Martínez, A.; Tejeda-Cruz, A.; Islas-Jácome, A.; González-Zamora, E.; Ibarra, I. A. Structure Stability of HKUST-1 towards Water and Ethanol and Their Effect on Its CO_2 Capture Properties. *Dalton Trans.* **2017**, *46*, 9192−9200.
(59) González-Martínez, G. A.; Zárate, J. A.; Martínez, A.; Sánchez-González, E.; Álvarez, J. R.; Lima, E.; González-Zamora, E.; Ibarra, I. A. Confinement of Alcohols to Enhance CO_2 Capture in MIL-53(Al). *RSC Adv.* **2017**, *7*, 24833−24840.
(60) Sánchez-González, E.; Mileo, P. G. M.; Álvarez, J. R.; González-Zamora, E.; Maurin, G.; Ibarra, I. A. Confined Methanol within InOF-1: CO_2 Capture Enhancement. *Dalton Trans.* **2017**, *46*, 15208−15215.
(61) Qian, J.; Jiang, F.; Yuan, D.; Wu, M.; Zhang, S.; Zhang, L.; Hong, M. Highly Selective Carbon Dioxide Adsorption in a Water-Stable Indium−Organic Framework Material. *Chem. Commun.* **2012**, *48*, 9696−9698.
(62) Vlugt, T. J. H.; García-Pérez, E.; Dubbeldam, D.; Ban, S.; Calero, S. Computing the Heat of Adsorption using Molecular Simulations: The Effect of Strong Coulombic Interactions. *J. Chem. Theory Comput.* **2008**, *4*, 1107−1118.
(63) Harris, J. G.; Yung, K. H. Carbon Dioxide's Liquid-Vapor Coexistence Curve and Critical Properties as Predicted by a Simple Molecular Model. *J. Phys. Chem.* **1995**, *99*, 12021−12024.
(64) Chen, B.; Potoff, J. L.; Siepmann, J. I. Monte Carlo Calculations for Alcohols and Their Mixtures with Alkanes. Transferable Potentials for Phase Equilibria. 5. United-Atom Description of Primary, Secondary, and Tertiary Alcohols. *J. Phys. Chem. B* **2001**, *105*, 3093−3104.
(65) Rappé, A. K.; Casewit, C. J.; Colwell, K. S.; Goddard, W. A., III; Skiff, W. M. UFF, a Full Periodic Table Force Field for Molecular Mechanics and Molecular Dynamics Simulations. *J. Am. Chem. Soc.* **1992**, *114*, 10024−10035.
(66) Mayo, S. L.; Olafson, B. D.; Goddard, W. A., III DREIDING: A Generic Force Field for Molecular Simulations. *J. Phys. Chem.* **1990**, *94*, 8897−8909.
(67) Zhao, X.; Xiao, B.; Fletcher, A. J.; Thomas, K. M.; Bradshaw, D.; Rosseinsky, M. J. Hysteretic Adsorption and Desorption of Hydrogen by Nanoporous Metal-Organic Frameworks. *Science* **2004**, *306*, 1012−1015.
(68) Choi, H. J.; Dincă, M.; Long, J. R. Broadly Hysteretic H_2 Adsorption in the Microporous Metal−Organic Framework Co(1,4-Benzenedipyrazolate). *J. Am. Chem. Soc.* **2008**, *130*, 7848−7850.
(69) Ibarra, I. A.; Yang, S.; Lin, X.; Blake, A. J.; Rizkallah, P. J.; Nowell, H.; Allan, D. R.; Champness, N. R.; Hubberstey, P.; Schröder, M. Highly Porous and Robust Scandium-Based Metal-Organic Frameworks for Hydrogen Storage. *Chem. Commun.* **2011**, *47*, 8304−8306.
(70) Nuñez, A. J.; Chang, M. S.; Ibarra, I. A.; Humphrey, S. M. Tuning the Host−Guest Interactions in a Phosphine Coordination Polymer through Different Types of Post-Synthetic Modification. *Inorg. Chem.* **2014**, *53*, 282−288.
(71) Ibarra, I. A.; MacE, A.; Yang, S.; Sun, J.; Lee, S.; Chang, J. S.; Laaksonen, A.; Schröder, M.; Zou, X. Adsorption Properties of MFM-400 and MFM-401 with CO_2 and Hydrocarbons: Selectivity Derived from Directed Supramolecular Interactions. *Inorg. Chem.* **2016**, *55*, 7219−7228.
(72) de Lange, M. F.; Verouden, K. J. F. M.; Vlugt, T. J. H.; Gascon, J.; Kapteijn, F. Adsorption-Driven Heat Pumps: The Potential of Metal−Organic Frameworks. *Chem. Rev.* **2015**, *115*, 12205−12250.
(73) Yang, R. T. *Gas Separation by Adsorption Processes*; Butterworth: Stoneham, 1987.
(74) Ibach, H. *Physics of Surfaces and Interfaces*; Springer: Berlin, 2006.
(75) Lemaire, E.; Decrette, A.; Bellat, J. P.; Simon, J. M.; Méthivier, A.; Jolimaître, E. Adsorption and Diffusion of Linear and Dibranched C_6 Paraffins in a ZSM-5 Zeolite. *Stud. Surf. Sci. Catal.* **2002**, *142*, 1571−1578.
(76) Tedds, S.; Walton, A.; Broom, D. P.; Book, D. Characterisation of Porous Hydrogen Storage Materials: Carbons, Zeolites, MOFs and PIMs. *Faraday Discuss.* **2011**, *151*, 75−94.
(77) Roque-Malherbe, R. M. A. *Adsorption and Diffusion in Nanoporous Materials*; CRC Press: Boca Raton, 2007.
(78) Miachon, S.; Syakaev, V. V.; Rakhmatullin, A.; Pera-Titus, M.; Caldarelli, S.; Dalmon, J. A. Higher Gas Solubility in Nanoliquids? *ChemPhysChem* **2008**, *9*, 78−82.
(79) Rakotovao, V.; Ammar, R.; Miachon, S.; Pera-Titus, M. Influence of the Mesoconfining Solid on Gas Oversolubility in Nanoliquids. *Chem. Phys. Lett.* **2010**, *485*, 299−303.
(80) Ho, L. N.; Clauzier, S.; Schuurman, Y.; Farrusseng, D.; Coasne, B. Gas Uptake in Solvents Confined in Mesopores: Adsorption versus Enhanced Solubility. *J. Phys. Chem. Lett.* **2013**, *4*, 2274−2278.

DOI: 10.1021/acs.jpcc.8b00215
J. Phys. Chem. C 2018, 122, 5566−5577

(81) Hu, Y.; Huang, L.; Zhao, S.; Liu, H.; Gubbins, K. E. Effect of Confinement in Nano-Porous Materials on the Solubility of a Supercritical Gas. *Mol. Phys.* **2016**, *114*, 3294−3306.
(82) Jiang, X.; Duan, H. B.; Khan, S. I.; Garcia-Garibay, M. A. Diffusion-Controlled Rotation of Triptycene in a Metal-Organic Framework (MOF) Sheds Light on the Viscosity of MOF-Confined Solvent. *ACS Cent. Sci.* **2016**, *2*, 608−613.

DOI: 10.1021/acs.jpcc.8b00215
J. Phys. Chem. C 2018, 122, 5566−5577